Biosensors and Bioelectronics 136 (2019) 31–37

Contents lists available at ScienceDirect

Biosensors and Bioelectronics

journal homepage: www.elsevier.com/locate/bios

A microRNA-triggered self-powered DNAzyme walker operating in living cells

Chang Liu, Yanlei Hu, Qingshan Pan, Jintao Yi, Juan Zhang, Manman He, Mengyun He, Tingting Chen**, Xia Chu*

State Key Laboratory of Chemo/Bio-Sensing and Chemometrics, College of Chemistry and Chemical Engineering, Hunan University, Changsha, 410082, PR China

ARTICLE INFO

Keywords:
DNAzyme-based walking machine
Intracellular miRNA-21
Gold nanoparticle

ABSTRACT

DNA-based nanomachines have received increasing attention due to their great potential to mimic natural biological motors and create novel modes of motion. Here, we report a DNAzyme-based walking machine, which can operate in living cells after triggered by intracellular miRNA-21. The walking machine is constructed by assembling DNAzyme walking strands and FAM-labeled substrate strands on a single gold nanoparticle (AuNP). The DNAzyme walking strand is first silenced by a blocker strand. After cellular uptake, DNAzyme-based walker can be triggered by intracellular miRNA-21 and autonomously walk along the AuNP-based 3D track fueled by DNAzyme-catalyzed substrate cleavage. Each walking step results in the cleavage of a substrate strand and the release of a FAM-labeled DNA strand, allowing real-time monitoring of the operation of the machine. The DNAzyme-based walking machine has been successfully applied to image and monitor miRNA-21 expression levels in living cells with excellent specificity and reliability. This walking machine would hold great potential in the miRNA associated biological research and disease diagnostics.

1. Introduction

MicroRNAs (miRNAs) are a family of single-stranded, a short length of 18–25 nucleotides, and non-coding RNA molecules that serve as critical regulators in cellular processes such as cell migration, proliferation, and apoptosis by regulating the gene expression (Dong et al., 2013). Lots of evidences have shown that the aberrant expression of miRNAs is related to occurrence, progression and metastasis of different cancers (Calin and Croce, 2006a,b). Due to the properties of regulating gene expression, miRNAs are considered to be significant biomarkers for disease diagnosis and prognosis, as well as potential targets for drug discovery and gene therapy (Kosaka et al., 2010). Therefore, the development of robust strategy to better monitor the miRNAs in living cells would be highly desirable.

To date, many detection methods have been developed for miRNAs analysis, such as microarray hybridization (Nelson et al., 2004), Northern blotting (Kim et al., 2010), and the real time polymerase chain reaction (PCR) (Li et al., 2009), amplified tandem Spinach-based aptamer transcription assay (AmptSpi assay) (Tang et al., 2018), and catalytic hairpin assembly (CHA) (Zhuang et al., 2014). Although these methods have been used for sensitive and high throughput detection of miRNAs in buffer or cell lysates, it is still a challenge to *in situ* visualize and monitor intracellular miRNAs owing to low expression level (less than 50000 copies per cell) and the complicated cell environments in living cells. Recently, a variety of nanomaterials, including two-dimensional materials (graphene oxide (Tang et al., 2015; Liu et al., 2016), and MnO_2 (Oudeng et al., 2018)), circular DNA stand (Tang et al., 2016), and zeolitic imidazolate framework-8 (Yi et al., 2017), and DNA nanoassembly (Z. Yang et al., 2018) have been explored for the detection of miRNAs in living cells. Despite very powerful, the development of other nanomaterials that integrate the ability of probe delivery with signal amplification function remains required.

Gold nanoparticles (AuNPs) possess the high DNA loading capacity (Zhang et al., 2012; Zeng et al., 2019) and excellent biocompatibility (Zhang et al., 2018). In 2007, Mirkin and co-workers first designed nanoflares to detect messenger RNA (mRNA) in living cells using the 13 nm Au NPs as an efficient probe delivery vehicle (Seferos et al., 2007). After that, Wright et al. reported hairpin DNA functionalized

* Corresponding author. State Key Laboratory of Chemo/Bio-Sensing and Chemometrics, College of Chemistry and Chemical Engineering, Hunan University, PR China.

** Corresponding author. State Key Laboratory of Chemo/Bio-Sensing and Chemometrics, College of Chemistry and Chemical Engineering, Hunan University, PR China.

E-mail addresses: chenting1104@hnu.edu.cn (T. Chen), xiachu@hnu.edu.cn (X. Chu).

https://doi.org/10.1016/j.bios.2019.04.031
Received 23 March 2019; Received in revised form 12 April 2019; Accepted 16 April 2019
Available online 19 April 2019
0956-5663/

AuNPs to *in situ* image the mRNA (Jayagopal et al., 2010). Tang et al. described a multicolor fluorescence nanoprobe based on AuNPs functionalized with three recognition sequences and three short dye-terminated reporter sequences (Li et al., 2012). Recently, further researches have also sought to apply the spherical DNA-AuNP conjugates for sensing intracellular miRNAs (He et al., 2016; Yang et al., 2017; Ye et al., 2017; Qian et al., 2016; Li et al., 2017). However, these nanoconjugates have been demonstrated to possess low hybridization efficiency between target and sensing probe because of the low expression level of miRNAs. Nowadays, more attentions have been focused on designing intelligent and highly efficient DNA nanomachine. Among these nanomachines, DNA-based walking machines with AuNP-constructed three-dimensional landscapes, which can convert chemical energy to mechanical motions, have attracted rapidly growing interest (Zhang et al., 2015; Qu et al., 2017; Yang et al., 2016; Chen et al., 2017; Wei et al., 2018; Lv et al., 2018). For example, Fan et al. reported an exonuclease III (Exo III)-powered stochastic DNA walker that can autonomously move on AuNP-based 3D track (Qu et al., 2017). However, this nanomachine needs exogenous additives such as Exo III to drive their motion, and restrains their potential applications in living cells. To solve this problem, some nanomachines have been modified to realize the operation in living cells. For instance, Yin et al. reported an entropy-driven DNA nanomachine for intracellular miRNA imaging (Liang et al., 2017). However, additional fuel strand must be introduced into living cells to release the walking strand. The authors subsequently improved the nanomachine by using endogenous ATP in cells to release the walking strand (Ma et al., 2018).

In this work, we developed a miRNA-triggered self-powered DNAzyme-based walking machine for miRNA imaging in living cells. DNAzymes can catalyze the cleavage of RNA or DNA molecules in a divalent cations-dependent manner. Currently, RNA-cleaving DNAzymes have obtained widespread applications in metal ions sensing, disease diagnostic and therapy (Wang et al., 2017; Zhou et al., 2017a,b; Wu et al., 2017; Zhou et al., 2017, 2017). Le et al. reported a DNAzyme-based intracellular motor, which was constructed by a long motor strand with a DNAzyme sequence and operated through the DNAzyme cleavage of the DNA-RNA chimeric substrates in the presence of cofactor Mn^{2+} (Peng et al., 2017). In addition, the DNAzyme-based walking machine that can move processively and autonomously along a one-dimensional track has also been studied in detail by Mao and Choi et al. (Cha et al., 2014, 2015; Tian et al., 2005). Currently, He et al. reported Mg DNAzyme-based walker could detect adenosine, Ag^{+}, and target DNA sequence in the solution not in living cells (K. Yang et al., 2018). So, such walking machine operating along the AuNP-based 3D track in living cells has never been reported. Here, we first attempt to design an intracellular miRNA-triggered DNAzyme-based walking machine. This machine possesses the following advantages: first, all components of the walking machine, including the walker and its track, are integrated onto a single AuNP, facilitating cellular uptake of the walking machine; second, the operation of the DNAzyme-based walker can be triggered by a specific molecule in the cell, for example, miRNA; third, the operation of the DNAzyme walker is self-powered, because the autonomous walking along the AuNP-based 3D track is fueled by DNAzyme-catalyzed substrate cleavage, avoiding the external addition of fuel strands or protein enzymes; finally, each walking step results in the cleavage of a substrate strand and the release of a fluorescently labeled DNA strand from the AuNP, allowing real-time monitoring of the operation of the machine.

2. Experimental section

The detailed description of chemicals and materials, apparatus, and synthesis of citrate capped AuNPs were supplied in Supplementary material (Please see Supplementary material).

2.1. Fabrication of DNA walking machine

Before mixing with as-prepared AuNPs, thiolated oligonucleotides were incubated with TCEP·HCl at a molar ratio of 1: 100 for 1 h in order to reduce the disulfide bond. For the preparation of blocker-DNAzyme double strands, 10 μL of 10 μM blocker was mixed with 8.35 μL of 10 μM DNAzyme in the 25 mM Tris-HCl (pH 7.4) with 137 mM NaCl at 37 °C for 2 h. The use of 1.2-fold molar excess of the blocker was to ensure the complete locking of the DNAzyme. After that, 125 μL fluorescence substrate (20 μM) and 20 μL prepared blocker-DNAzyme double strands (4.175 μM), were added to the 500 μL AuNPs (10 nM) and shaken overnight, which at the molar ratio of 500: 16.7: 1. After 16 h, 25 μL of 1% Tween 20 was added to the above solution. Then, 74 μL of 0.1 M phosphate buffer (pH 7.4) was added to the above mixture to reach a 0.01 M phosphate concentration. The salt concentration of the mixture was slowly increased to 0.3 M NaCl over an 8 h period by adding the NaCl solution (2 M) four times. To remove the excess DNA, the resulting solution was centrifuged (13000 rpm, 30 min) and then washed three times and stored in the 25 mM Tris-HCl (pH 7.4) with 137 mM NaCl.

2.2. Determination of substrate loading on AuNPs

The DTT was used to release the substrates from the AuNPs for determining the substrate loading on each AuNP. In detail, 10 μL of 10 nM nanomachine was mixed with 10 μL of 100 mM DTT, the mixture was then diluted to 100 μL by using 1 × PBS buffer and shaken overnight at room temperature. The released substrates were separated via centrifugation and the substrate loading amount was determined by fluorescence measurements and compared with a standard curve of FAM-labeled substrate.

2.3. PAGE electrophoresis

In the gel electrophoresis assay, all samples were prepared in advance. For example, 7 μL of the 25 mM Tris-HCl buffer (with 137 mM NaCl, pH 7.4) containing blocker1 (3.14 μM) and DNAzyme (2.86 μM) were incubated at 37 °C for 2 h. Then, the above solution of blocker1-DNAzyme double strands was incubated with 1 μL miRNA-21 target (22 μM), 1 μL substrate (20 μM) and 1 μL 7500 μM Mn^{2+}. After incubation at 37 °C for 3 h, the final mixture was incubated with 2 μL of 6 × loading buffers and fixed on the 20% native page gel (lane 12).

2.4. Assessment of the miRNA-triggered DNAzyme walker operation

To evaluate the DNAzyme walker operation triggered by miRNA-21, we monitored the sample fluorescence increase in real-time detection. Briefly, 100 μL of the 2.5 nM AuNPs were incubated with different concentrations of miRNA-21 in 25 mM Tris-HCl buffer containing 137 mM NaCl and 750 μM $MnCl_2$.

2.5. Cell culture

MCF-7 and HeLa cells were cultured in RPMI-1640 medium with 10% fetal bovine serum (FBS), streptomycin (100 μg ml^{-1}), and penicillin (100 units mL^{-1}). MCF-10a cells were cultured in DMEM/F12 with 5% horse serum, 50 μg ml^{-1} Penicillin-Streptomycin (P/S), 100 ng ml^{-1} cholera toxin, 10 μg ml^{-1} insulin, 0.5 μg ml^{-1} hydrocortisone and 20 ng ml^{-1} hEGF. All cell lines were maintained at 37 °C in a humidified atmosphere containing 5 wt %/vol CO_2.

2.6. Fluorescence imaging upon the operating of the miRNA-triggered DNAzyme-based walking machine in living cells

The cells were incubated with 1 mL of culture medium containing 2.5 nM DNA-functionalized AuNPs and 250 μM Mn^{2+} at 37 °C for 6 h.

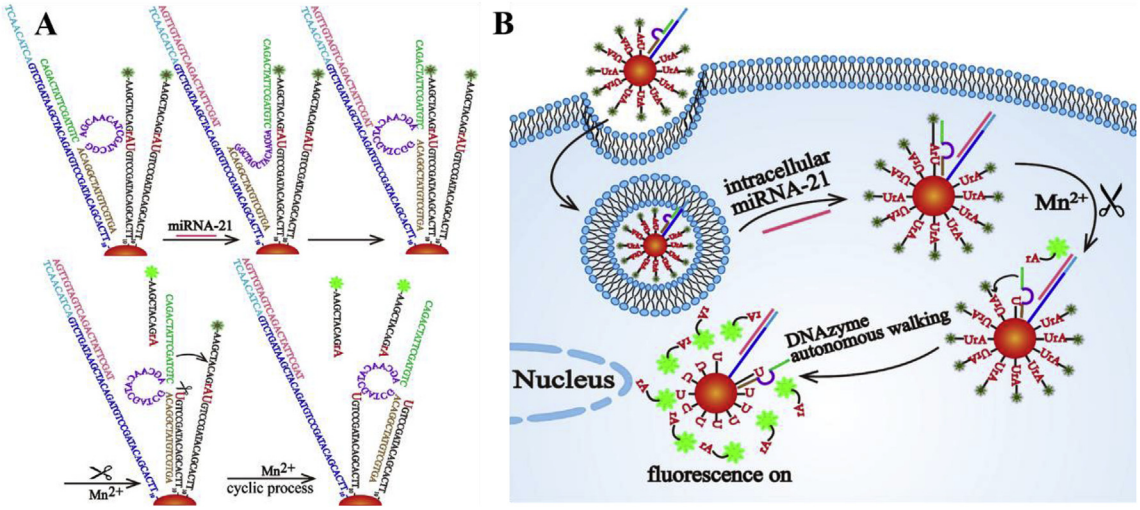

Scheme 1. Schematic illustration of the operation of the miRNA-triggered self-powered DNAzyme walker.

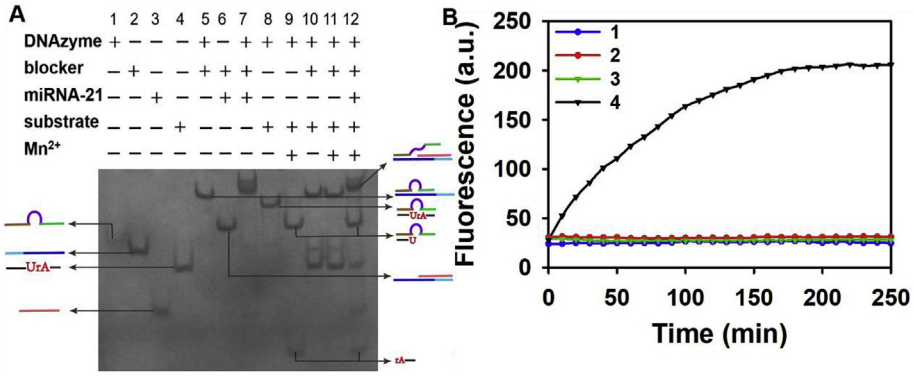

Fig. 1. (A) PAGE gel electrophoresis image. (B) Real-time monitoring of fluorescence generated by 2.5 nM DNA-functionalized AuNPs (blue); 2.5 nM DNA-functionalized AuNPs with 35 nM miRNA-21 (red); 2.5 nM DNA-functionalized AuNPs with 750 μM Mn^{2+} (green); 2.5 nM DNA-functionalized AuNPs with 35 nM miRNA-21 and 750 μM Mn^{2+} (black). (For interpretation of the references to color in this figure legend, the reader is referred to the Web version of this article.)

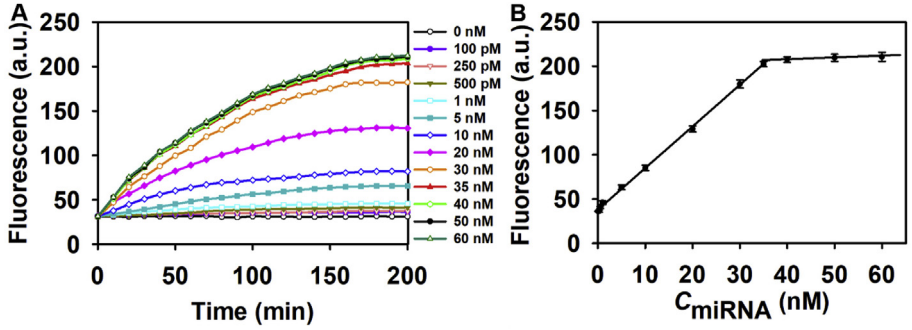

Fig. 2. (A) Real-time fluorescence changes with time of 2.5 nM DNA-functionalized AuNPs responding to the different miRNA-21 concentrations in the presence of 750 μM Mn^{2+}. (B) Correlation curve of fluorescence intensities at 3 h versus varying concentrations of the miRNA-21.

Then, the cells were washed three times with cold PBS before imaging. The experiments in which miRNA-21 expression fluctuations in living cells were performed as follows: HeLa cells were first transfected with 0.2 mM MicrONhsa-miR-21-5p mimic or 0.5 mM MicrOFFhsa-miR-21-5p inhibitor using 6 μL of transfection reagent in 1 mL culture medium at 37 °C for 24 h. Then the cells were incubated with 1 mL of culture medium containing 2.5 nM DNA-functionalized AuNPs and 250 μM Mn^{2+} at 37 °C for 6 h. All fluorescence images were acquired using an oil dipping objective (100 ×, 1.25 NA) on a Nikon confocal laser scanning fluorescence microscope.

3. Results and discussion

3.1. Design principle of the walking machine

The strategy of the miRNA-triggered self-powered DNAzyme walking machine is presented in Scheme 1. The walking machine is composed of a small number of DNAzyme walking strands and abundant fluorescently labeled DNA-RNA chimera substrate strands, and both of the two components are integrated onto a single AuNP surface through Au—S bond assembly. The DNAzyme walking strand is first silenced by a blocker strand. After cellular uptake of the nanomachine, the operation of the DNAzyme walker could be initiated by endogenous miRNA-21, which could embed in blocker strand through a 9 nt toehold at the 5' end. The upper leg of the DNAzyme walker becomes unbound,

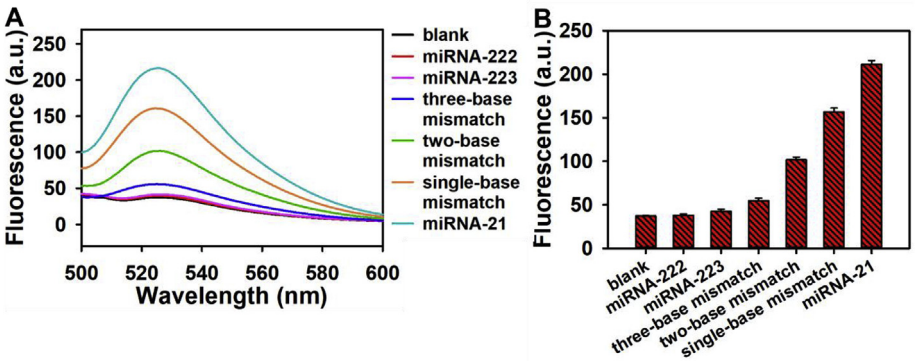

Fig. 3. Specificity of the DNAzyme-based walking machine. (A) Fluorescence spectra and (B) the fluorescence intensity of the walking machine initiated by different triggers. The concentrations of the triggers were 35 nM.

and the unpaired upper leg then binds to the adjacent FAM-labeled DNA-RNA chimera substrate strand through Watson-Crick base-pairing. Subsequently, the low leg migrates to the upper leg-bound substrate strand by a single step of pseudo-continuous transition (Tian et al., 2005; Zhang and Seelig, 2011). In the presence of Mn^{2+}, the DNAzyme cleaves its substrate into two fragments. Because of the relatively weak affinity between the short upper fragment of the substrate and the DNAzyme, the upper leg of the DNAzyme walker becomes free and unbound again, resulting in the release of the short upper fragment of the substrate. Then, the DNAzyme walker moves from one substrate to the next cycle of substrate binding, cleavage, and dissociation, completing a single turnover. Each walking step of the nanomachine results in the release of a fluorescently labeled DNA strand from the AuNP, allowing real-time monitoring of the operation of the machine.

3.2. Characterization of nanomachine

The bare AuNPs and the DNA-functionalized AuNPs were characterized by TEM. The TEM images showed that the DNA-modified AuNPs had an average size about 14.5 ± 0.2 nm, slightly larger than that of bare AuNPs (13 nm ± 0.3 nm) (Fig. S1 A, B). The UV–vis absorption spectra of the bare AuNPs exhibited the characteristic peaks of AuNPs at 519 nm (Fig. S1 C). After functionalized with a dense monolayer of DNA strands, the absorption peak of the nanomachine showed a tiny red shift (~3 nm) to 522 nm. The zeta potential (Fig. S1 D) shifted from −36.3 to −47.0 mV and DLS measurements (Fig. S1 E, F) showed an increase in the average hydrodynamic diameter (from 11.9 ± 3.0 nm to 19.3 ± 5.7 nm) after functionalized with DNA strands. These results strongly demonstrated that the DNA strands had been successfully modified on the surface of the AuNPs.

3.3. Operation of the walking machine in vitro

To investigate whether the design of the walking machine is feasible, the gel electrophoresis assay was first carried out. As shown in Fig. 1A, the substrate strands could be cleaved by DNAzyme strands in the presence of Mn^{2+}, releasing a very short fragment (the bottom band in Fig. 1A, lane 9). However, when the DNAzyme strand hybridized beforehand with a blocker strand, the substrate strands would not be cleaved even in the presence of Mn^{2+}, as demonstrated by the absence of the bottom band in Fig. 1A, lane 11. This result implied that the DNAzyme walking strand could be silenced effectively by the blocker strand. When the target miRNA-21 was introduced in the system, a bottom band corresponding to the very short cleavage product could be observed in Fig. 1A, lane 12. The result suggested that the miRNA-21 target could trigger the release of the DNAzyme walking strand by hybridization with the blocker strand and realize the cleavage of the substrate.

We then assembled the DNAzyme walking strands and fluorescently labeled substrate strands to AuNP surface and investigated the operation of the walking machine using fluorescence experiment. When the miRNA-21 target was introduced to the system with Mn^{2+}, the fluorescence increased significantly with time and reached a maximum signal at 3 h, and a ratio of signal to background as high as 6.0 could be obtained (Fig. 1B, black curve). This result suggested that the DNAzyme walking strand could be activated effectively by hybridization between the blocker strands with the miRNA-21 target and then triggered autonomous walking along AuNP-based 3D track.

Next, we optimized several operating conditions of the DNAzyme walking machine to obtain an optimal walking efficiency. We first investigated the concentration of Mn^{2+} for the operation of the walking machine (Fig. S2). The result showed that the Mn^{2+} concentration of 750 μM was best for fueling the walking of the nanomachine. We also studied the effect of the length of the substrate, 7–16 nt and 9–16 nt (the upper-low leg lengths of the FAM-labeled substrate strand as indicated in Fig. S3), on the walking efficiency. Compared with 7–16 substrate strands, the 9–16 substrate strands gave relatively high walking efficiency. This may be the 9 nt toehold has relatively high hybridization efficiency and facilitates the migration of the walking strand. Furthermore, the ratio of the DNAzyme walking strands to substrate strands modified on the AuNP surface was also investigated. The result revealed that the ratio of 1:30 was best, corresponding to approximate 93 FAM-labeled DNA-RNA chimera substrate strands and 3 DNAzyme walking strands on a single AuNP (Fig. S4).

Under the optimal operation conditions, we further investigated the operation of the DNAzyme-based walking machine triggered by the varying concentrations of miRNA-21 target. The fluorescence signal increased gradually with time and reached a maximal value at about 3 h (Fig. 2A). The fluorescence intensities at 3 h increased with the increasing concentrations of the target miRNA-21 from 0 to 60 nM. The fluorescence intensities correlated linearly with the miRNA-21 concentrations in the range from 100 pM to 35 nM (Fig. 2B), and the detection limit was estimated to be 34 pM (in terms of the rule of 3 times deviation over the blank response). Compared with other methods for miRNA detection, this walking machine showed a comparable detection limit (Table S2).

To confirm that the DNAzyme-based walking machine was specifically activated by the target miRNA-21, we examined two other miRNAs and three variants with one, two or three mismatched bases. As shown in Fig. 3, no significant fluorescence increase was observed after addition of other non-target miRNAs. The single-base and two-base mismatched DNA strand interfered with the detection of miRNA-21 target. However, almost no significant influence was observed for three-base mismatched DNA strand. Altogether, the walking machine provided a good selectivity for miRNA-21 detection.

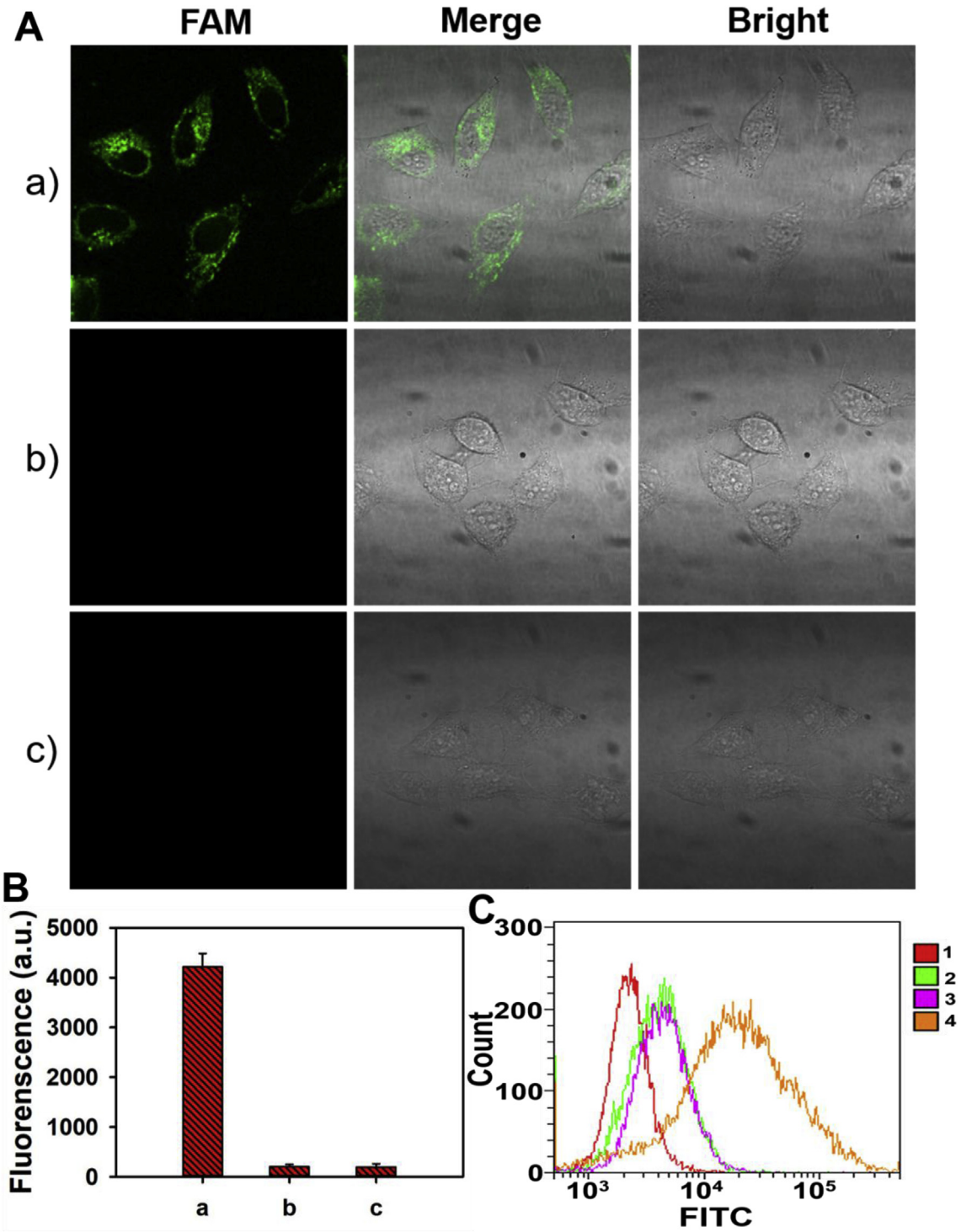

Fig. 4. Operation of the walking machine in HeLa cells. (A) Fluorescence microscopy images of HeLa cells treated with (a) DNAzyme-based walking machine and 250 μM Mn^{2+}, (b) DNAzyme-based walking machine only, (c) nonspecific walking machine and 250 μM Mn^{2+}. (B) Average fluorescence intensity of the HeLa imaging with above different treatment. (C) Flow cytometric assay of (1) HeLa cells, (2) HeLa cells treated with DNAzyme-based walking machine only, (3) HeLa cells treated with nonspecific walking machine and 250 μM Mn^{2+}, (4) HeLa cells treated with DNAzyme-based walking machine and 250 μM Mn^{2+}.

3.4. Operation of the walking machine in living cells

First, we evaluated the cytotoxicity of the DNAzyme-based walking machine using MTT assays (Fig. S5). The high viability of the cells (> 81%) was obtained even after incubated with 7.5 nM AuNPs for 24 h, implying the low cytotoxicity of our walking machine.

Next, we test the intracellular operation of our walking machine triggered by the miRNA-21 target. After incubation with DNA-functionalized AuNPs (2.5 nM) and Mn^{2+} (250 μM) for 6 h, HeLa cells gave bright green fluorescence (Fig. 4A a, B), suggesting that the DNAzyme-based walking machine successfully operated in living cells. When the cells were not treated Mn^{2+}, no fluorescence was observed (Fig. 4A b, B), confirming that the substrate strands on the AuNPs were stable. In addition, we introduced the mismatched bases at the 9 nt toehold of the blocker strand to construct a nonspecific walking machine. No fluorescence signal was observed (Fig. 4A c, B). This result

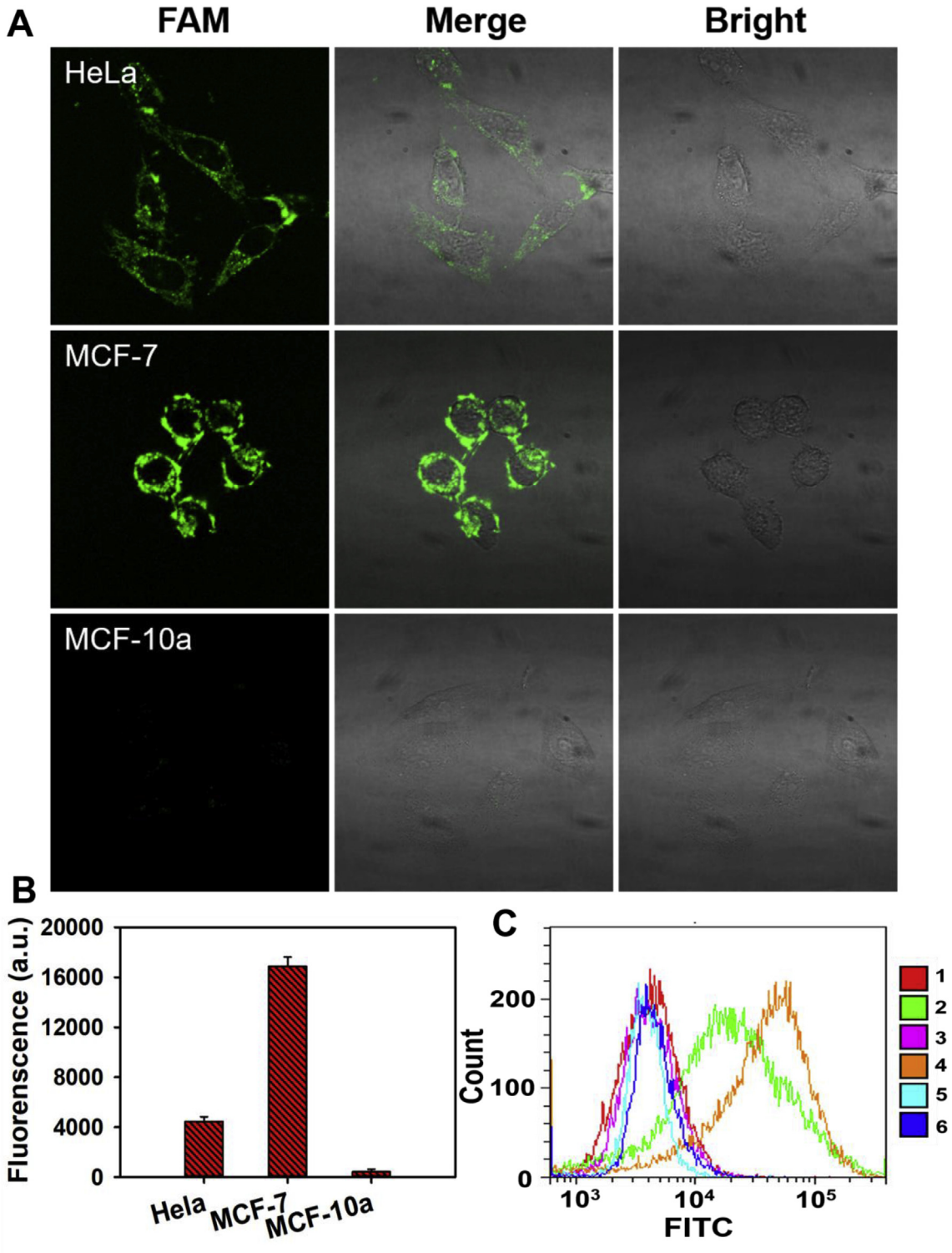

Fig. 5. Operation of the walking machine in different types of cell lines including HeLa, MCF-7 and MCF-10a cells. (A) Fluorescence images of HeLa, MCF-7 and MCF-10a cells after incubated with the 2.5 nM DNA-functionalized AuNPs and 250 μM Mn^{2+}. (B) Average fluorescence intensity of the three different cell lines imaging. (C) Flow cytometry analysis of (1) HeLa, (3) MCF-7, and (5) MCF-10a cells incubated with the walking machine; and the (2) HeLa, (4) MCF-7, and (6) MCF-10a cells incubated with the walking machine and Mn^{2+}.

indicated that the DNAzyme walking strand could not be activated effectively because the blocker strand was not complementary with the miRNA-21. These results were also confirmed by corresponding flow cytometric assay (Fig. 4C). Therefore, this walking machine could operate effectively in living cells with excellent specificity and reliability. In addition, the co-localization analysis with lysosome indicated that most green fluorescence signals distributed in cytoplasm (Fig. S6).

Next, we explored the optimal operating conditions of the intracellular walking machine by treating HeLa cells with different concentrations of AuNPs and Mn^{2+}.We also observed that 2.5 nM DNA-functionalized AuNPs and 250 μM Mn^{2+} was enough for the operation of the walking machine in cells (Figs. S7 and 8). Higher Mn^{2+}

concentrations would induce obvious cytotoxicity.

We further investigate the operation of the machine in other types of cell lines. As shown in Fig. 5A and B, the MCF-7 cells showed the brightest fluorescence signal, followed by HeLa cells, and the weakest fluorescence was observed in the MCF-10a cells, indicating that MCF-7 cells gave the highest expression level of miRNA-21, whereas MCF-10a cells had the lowest expression. These observations were further confirmed by corresponding flow cytometric assay (Fig. 5C), and qRT-PCR experiments (Fig. S9). All results revealed that our DNAzyme-based walking machine could distinguish the different miRNA-21 expression in living cells, exhibiting the good applicability for intracellular miRNA-21 imaging.

Finally, we interrogated the utility of the walking machine to probe the fluctuation of miRNA-21 expression levels in HeLa cells. Compared with the untreated HeLa cells, the cells treated by the miRNA-21 mimic (Leone et al., 2013) were observed brighter FAM fluorescence, whereas the cells incubated with the miRNA-21 inhibitor (Leone et al., 2013) appeared weaker fluorescence (Figs. S10A and B). Furthermore, these fluorescence imaging results were consistent with those obtained by the corresponding flow cytometric assay (Fig. S10C) and qRT-PCR experiments (Fig. S11). These results imply that our walking machine holds great potential in the miRNA associated biological research.

4. Conclusions

In summary, we developed a miRNA-triggered self-powered DNAzyme-based walking machine and applied it to specifically image of miRNA in living cells. The DNAzyme-based walking machine integrated DNAzyme walker and its track onto a single AuNP, facilitating cellular uptake. Importantly, no need of the external addition of fuel strands or protein enzymes, the DNAzyme-based walker was self-powered and could walk along the AuNP-based 3D track after triggered by intracellular specific miRNA, releasing a fluorescently labeled DNA strand to monitor the operation of the walker. The DNAzyme-based walking machine showed the excellent specificity and reliability to the intracellular miRNA imaging. To our knowledge, this is the first DNAzyme-based walking machine operating in living cells. It would hold great potential in the miRNA associated biological research and disease diagnostics.

CRediT authorship contribution statement

Chang Liu: Investigation, Writing - original draft. **Yanlei Hu:** Conceptualization, Writing - review & editing. **Qingshan Pan:** Conceptualization, Writing - review & editing. **Jintao Yi:** Formal analysis. **Juan Zhang:** Formal analysis. **Manman He:** Formal analysis. **Mengyun He:** Data curation. **Tingting Chen:** Methodology, Supervision. **Xia Chu:** Methodology, Supervision.

Acknowledgments

This work was supported by the National Natural Science Foundation of China (No. 21525522 and 21705039), the Foundation for Innovative Research Groups of NSFC (Grant 21521063) and project funded by China Postdoctoral Science Foundation (2017M620343).

Appendix A. Supplementary data

Supplementary data to this article can be found online at https://doi.org/10.1016/j.bios.2019.04.031.

References

Calin, G., Croce, C., 2006a. Nat. Rev. Canc. 6, 857–866.
Calin, G., Croce, C., 2006b. Cancer Res. 66, 7390–7394.
Chen, J., Zuehlke, A., Deng, B., Peng, H., Hou, X., Zhang, H., 2017. Anal. Chem. 89, 12888–12895.
Cha, T., Pan, J., Chen, H., Salgado, J., Li, X., Mao, C., Choi, J., 2014. Nat. Nanotechnol. 9, 39–43.
Cha, T., Pan, J., Chen, H., Robinson, H., Li, X., Mao, C., Choi, J., 2015. J. Am. Chem. Soc. 137, 9429–9437.
Dong, H., Lei, J., Ding, L., Wen, Y., Ju, H., Zhang, X., 2013. Chem. Rev. 113, 6207–6233.
He, X., Zeng, T., Li, Z., Wang, G., Ma, N., 2016. Angew. Chem. Int. Ed. 128, 3073–3076.
Jayagopal, A., Halfpenny, K., Perez, J., Wright, D., 2010. J. Am. Chem. Soc. 132, 9789–9796.
Kosaka, N., Iguchi, H., Ochiya, T., 2010. Cancer Sci. 101, 2087–2092.
Kim, S., Li, Z., Moore, P., Monaghan, A., Chang, Y., Nichols, M., John, B., 2010. Nucleic Acids Res. 38 e98-e98.
Li, J., Yao, B., Huang, H., Wang, Z., Sun, C., Fan, Y., Chang, Q., Li, S., Wang, X., Xi, J., 2009. Anal. Chem. 81, 5446–5451.
Liu, H., Tian, T., Ji, D., Ren, N., Ge, S., Yan, M., Yu, J., 2016. Biosens. Bioelectron. 85, 909–914.
Li, N., Chang, C., Pan, W., Tang, B., 2012. Angew. Chem. Int. Ed. 51, 7426–7430.
Li, D., Zhou, W., Yuan, R., Xiang, Y., 2017. Anal. Chem. 89, 9934–9940.
Liang, C., Ma, P., Liu, H., Guo, X., Yin, B., Ye, B., 2017. Angew. Chem. Int. Ed. 56, 9077–9081.
Leone, E., Morelli, E., Martino, M., Amodio, N., Foresta, U., Gulla, A., Rossi, M., Neri, A., Giordano, A., Munshi, N., Anderson, K., Tagliaferri, P., Tassone, P., 2013. Clin. Cancer Res. 19, 2096–2106.
Lv, S., Zhang, K., Zeng, Y., Tang, D., 2018. Anal. Chem. 90, 7086–7093.
Ma, P., Liang, C., Zhang, H., Yin, B., Ye, B., 2018. Chem. Sci. 9, 3299–3304.
Nelson, P., Baldwin, D., Scearce, L., Oberholtzer, J., Tobias, J., Mourelatos, Z., 2004. Nat. Methods 1, 155–161.
Oudeng, G., Au, M., Shi, J., Wen, C., Yang, M., 2018. ACS Appl. Mater. Interfaces 10, 350–360.
Peng, H., Li, X., Zhang, H., Le, X., 2017. Nat. Commun. 8, 14378–14390.
Qian, R., Cao, Y., Long, Y., 2016. Anal. Chem. 88, 8640–8647.
Qu, X., Zhu, D., Yao, G., Su, S., Chao, J., Liu, H., Zuo, X., Wang, L., Shi, J., Wang, L., Huang, W., Pei, H., Fan, C., 2017. Angew. Chem. 129, 1881–1884.
Seferos, D., Giljohann, D., Hill, H., Prigodich, A., Mirkin, C., 2007. J. Am. Chem. Soc. 129, 15477–15479.
Tang, X., Deng, R., Sun, Y., Ren, X., Zhou, M., Li, J., 2018. Anal. Chem. 90, 10001–10008.
Tang, L., Ying, W., Li, J., 2015. Chem. Soc. Rev. 44, 6954–6980.
Tang, Y., Wang, T., Chen, M., He, X., Feng, X., 2016. Biosens. Bioelectron. 85, 151–156.
Tian, Y., He, Y., Chen, Y., Yin, P., Mao, C., 2005. Angew. Chem. Int. Ed. 44, 4355–4358.
Wei, W., Wei, M., Yin, L., Pu, Y., Liu, S., 2018. Microchim. Acta 185 494-494.
Wang, W., Satyavolu, N., Wu, Z., Zhang, J., Zhu, J., Lu, Y., 2017. Angew. Chem. Int. Ed. 129, 6798–6802.
Wu, Z., Fan, H., Satyavolu, N., Wang, W., Lake, R., Jiang, J., Lu, Y., 2017. Angew. Chem. Int. Ed. 56, 8721–8725.
Yi, J., Chen, T., Huo, J., Chu, X., 2017. Anal. Chem. 89, 12351–12359.
Yang, Z., Zhang, S., Zhao, H., Niu, H., Wu, Z., Chang, H., 2018. Anal. Chem. 90, 13891–13899.
Yang, Y., Huang, J., Yang, X., He, X., Quan, K., Xie, N., Ou, M., Wang, K., 2017. Anal. Chem. 89, 5850–5856.
Yang, K., Wang, H., Ma, N., Zeng, M., Luo, H., He, D., 2018. ACS Appl. Mater. Interfaces 10, 44546–44553.
Ye, S., Li, X., Wang, M., Tang, B., 2017. Anal. Chem. 89, 5124–5130.
Yang, X., Tang, Y., Mason, S., Chen, J., Li, F., 2016. ACS Nano 10, 2324–2330.
Zhang, H., Lai, M., Peng, H., Li, X., Le, X., 2015. Angew. Chem. Int. Ed. 54, 14326–14330.
Zhang, D., Seelig, G., 2011. Nat. Chem. 3, 103–113.
Zhang, B., Liu, B., Tang, D., Niessner, R., Chen, G., Knopp, D., 2012. Anal. Chem. 84, 5392–5399.
Zhang, K., Lv, S., Lin, Z., Li, M., Tang, D., 2018. Biosens. Bioelectron. 101, 159–166.
Zeng, R., Zhang, L., Su, L., Luo, Z., Zhou, Q., Tang, D., 2019. Biosens. Bioelectron. 133, 100–106.
Zhou, W., Saran, R., Liu, J., 2017a. Chem. Rev. 117, 8272–8325.
Zhou, W., Ding, J., Liu, J., 2017b. Theranostics 7, 1010–1025.
Zhuang, J., Lai, W., Chen, G., Tang, D., 2014. Chem. Commun. 50, 2935–2938.